Self-Adhesion of Polyethylene in the Melt. 2. Comparison of Heterogeneous and Homogeneous Copolymers

N. Z. Qureshi,[†] M. Rogunova,[†] E. V. Stepanov,[†] G. Capaccio,[‡] A. Hiltner,*[,†] and E. Baer[†]

Department of Macromolecular Science and Center for Applied Polymer Research, Case Western Reserve University, Cleveland, Ohio 44106-7202, and BP Amoco Chemicals, Applied Technology, Grangemouth, FK3 9XH, U.K.

Received March 31, 2000; Revised Manuscript Received January 17, 2001

ABSTRACT: The unexpectedly long time scale for development of melt adhesion strength in blown films of molecularly heterogeneous Ziegler−Natta ethylene copolymers previously led to speculation on the existence of a surface layer enriched in low molecular weight, highly branched fractions. In the present study the hypothesis was tested by performing the same melt adhesion experiments on metallocene ethylene copolymers. These copolymers should not develop a surface layer because the chains are homogeneous in branch content and the molecular weight distribution is relatively narrow. Melt adhesion of heterogeneous and homogeneous ethylene copolymers was strikingly different. Whereas the time dependence for melt adhesion of heterogeneous copolymers was 2 orders of magnitude longer than the time for complete interdigitation of the surface chains, ascribed to the presence of a surface layer that needed to resolve in order for bulk chains to reach the interface and for maximum adhesion strength to develop, full adhesion of homogeneous copolymers was achieved instantly on the experimental time scale. Furthermore, homogeneous copolymers could exhibit an order of magnitude higher peel strength in the melt due to the possibility for strain-induced crystallization. Tapping mode atomic force microscopy (AFM) confirmed the existence of an amorphous surface layer on heterogeneous copolymers. By probing to a maximum depth of 30−40 nm, as determined by the force-probe method, the AFM tip did not penetrate through the amorphous layer, which was previously estimated to be about 100 nm thick. In contrast, the surface of homogeneous copolymers exhibited the same densely packed lamellar morphology as the bulk. The amorphous surface layer of heterogeneous copolymers was replicated by blending homogeneous copolymers of different branch content. The blends reproduced the major melt adhesion characteristics of heterogeneous copolymers.

Introduction

Self-adhesion in the melt is an intrinsic type of adhesion for polymers. Developed through mutual diffusion and interdigitation of interfacial chains, self-adhesion is directly related to the molecular composition of the material.[1,2] Fundamental studies of self-adhesion usually focus on correlations with average molecular characteristics. The role of molecular heterogeneity, which is intrinsic to most synthetic polymers, is not well understood. However, this aspect is particularly relevant to the large class of ethylene copolymers where structural heterogeneity takes the form of excessive concentration of short chain branches on highly mobile chains of low molecular weight.[3]

Molecular heterogeneity can impact on development of self-adhesion through several mechanisms. It is known from studies of adhesion in monodisperse species that both the dynamics of surface chain interdigitation and the maximum adhesion (cohesive strength) depend strongly on molecular weight.[1,2] A recent investigation of interdiffusion kinetics in microlayers of highly polydisperse polyethylenes revealed the time scale for consecutive participation of different molecular weight fractions in interfacial mass transfer.[4,5] This demonstrated the potential for molecular weight distribution to control the time dependence of adhesion strength. The same study indicated that branching decreases the interdiffusion rate. Nevertheless, the effect of short-chain branching on chain reptation dynamics has been largely neglected, despite the common use of hydrogenated polybutadienes in experimental studies of adhesion and interdiffusion.[6−8] Other effects arising from differences in interaction between chains with high and low branch content are expected. These differences are known to cause phase separation of monodisperse fractions extracted from a typical heterogeneous polyethylene.[9,10]

Another consequence of molecular heterogeneity is the possibility for the composition of chains near the surface to differ from the average composition. Segregation of low molecular weight chains to the surface is well-known and exists even for linear homopolymers.[2,11] Qualitatively, the driving force for segregation is of both entropic and enthalpic origin. The entropic reason for segregation is halving in the conformational freedom of polymer chains on the surface compared to chains in the bulk. Thus, locating chains on the surface is not profitable in terms of thermodynamic free energy. However, the shorter the chain, the less freedom it has and, hence, the less entropy is lost if this chain is located on the surface. The enthalpic reason for segregation is the decrease in surface energy due to the interaction of chain ends. Shorter chains have a higher concentration of chain ends per unit volume. The enthalpic advantage for surface segregation can be considerably enhanced by changing the chain topology to increase the concentration of chain ends, for example, by mixing linear chains with stars or brushes of the same backbone structure.[11−13]

[†] Case Western Reserve University.
[‡] BP Amoco Chemicals.
* Corresponding author.

10.1021/ma000584p CCC: $20.00
Published on Web 03/20/2001

Table 1. Copolymer Characterization

polymer designation	comonomer	density (g cm^{-3})	avg branch conc[a] (per 1000C)	M_w[a] (kg mol^{-1})	M_w/M_n[a]	ΔH (J g^{-1})	T_m (°C)
C4	butene	0.9193	~20	118	4.0	134	123
C6	hexene	0.9169	~20	118	3.7	128	125
4MP1	4-methyl-pentene-1	0.9167	~20	111	3.6	136	126
*m*C6	hexene	0.9200	~10	96	2.1	122	117
*m*C8-87	octene	0.8732	~62	132[b]	2.0	42	40−70
*m*C8-91	octene	0.9149	~14	125[b]	2.0	146	115

[a] Provided by the manufacturer. [b] *m*C8-87: $I_2 = 0.8$; *m*C8-87: $I_2 = 1.0$.

Introduction of short-chain branches by copolymerization of ethylene with an α-olefin increases the effective number of chain ends proportionally to the comonomer content. It is well-known that linear low-density polyethylenes produced by conventional Ziegler−Natta catalysts are characterized by a wide molecular weight distribution and considerable nonuniformity in comonomer distribution. Furthermore, the chains with highest concentration of short-chain branches are also those in the low molecular weight tail of the molecular weight distribution.[3] Consequently, short chains that are driven to the surface by the entropic contribution to the chemical potential also have an enthalpic advantage in moving to the surface. In very thin films prepared from model blends of polyolefins, dramatic surface enrichment by a highly branched component is well established.[14,15]

Experimental investigation of these effects requires a technique for consecutively sealing and peeling film specimens at the same temperature, above the melting point. Methodology developed in a preceding study made possible the first direct measurements of melt adhesion in a wide range of temperatures, sealing times, and peeling rates.[16] Taking advantage of the new experimental technique, the molecular mechanisms and kinetics of adhesion in a group of short-chain branched linear polyethylenes with broad molecular weight distribution were explored. It was found that the adhesive strength increased with the contact time in accordance with the conventional $t^{1/2}$ dependence until saturation at the maximum strength. However, the saturation time in all cases was 2 orders of magnitude longer than the time for complete interdigitation of surface chains. This was ascribed to the presence of an amorphous layer on the free surface that was thought to originate from surface segregation of the lower molecular weight, higher branch content fractions. The layer, doubled upon sealing, needed to resolve in order for long chains from the bulk to reach the interface and maximum adhesion strength to develop. Estimates based on interdiffusion kinetics gave a thickness of 200 nm for the doubled layer.

The hypothesis of a surface layer on heterogeneous ethylene copolymers can be tested by comparison with the melt adhesion of metallocene copolymers, which have homogeneous comonomer content distribution and narrower molecular weight distribution. The postulated surface layer should not exist in these materials. Accordingly, the melt adhesion should reach the maximum strength instantaneously on the experimental time scale. Furthermore, the surface layer can be experimentally modeled by blending metallocene copolymers of different comonomer content in either miscible or immiscible compositions. The experimental procedure previously developed for consecutively sealing and peeling a polymeric film at the same temperature above the melting point is used to address these issues.

Experimental Section

Materials. Four ethylene copolymers were provided by BP Amoco Chemicals as pellets and as blown films 50 μm thick (Table 1). Three of the copolymers were produced with a conventional Ziegler−Natta catalyst using comonomers butene (C4), 4-methylpentene-1 (4MP1), and hexene (C6). These copolymers were characterized by nonuniform comonomer placement. Temperature rising elution fractionation (TREF) curves revealed two peaks in the short-chain branch distribution: a large peak containing fractions with higher branch concentrations and a smaller peak consisting of fractions with lower branch concentrations.[16] The main peak was much larger for the C4 copolymer than for the 4MP1 and C6 copolymers. The second peak, which corresponded to chains with longer methylene sequences, was prominent in the curves of the 4MP1 and C6 copolymers. This peak was much smaller, almost a shoulder, in the curve of the C4 copolymer. Furthermore, the tail in the distribution extended to longer methylene sequence lengths for the 4MP1 and C6 copolymers than for the C4 copolymer. The TREF curves suggested that the C4 copolymer was more homogeneous in its branch distribution than the C6 and 4MP1 copolymers.

The fourth copolymer was produced with a metallocene catalyst with hexane as the comonomer (*m*C6) and was also provided as blown film 50 μm thick (Table 1). It was characterized by homogeneous comonomer placement. The material had the same density as the heterogeneous copolymers but lower branch content. The four copolymers provided by BP Amoco Chemicals were of similar average molecular weight; the homogeneous copolymer had a narrower molecular weight distribution.

Two homogeneous copolymers with octene as the comonomer were obtained from The Dow Chemical Company. The copolymers, designated *m*C8-91 and *m*C8-87, were similar in molecular weight but differed in comonomer content (Table 1). Binary blends of *m*C8-91 with 5, 10, 20, 30, and 50 vol % *m*C8-87 were prepared by melt blending. The dry blends were processed in a Haake Rheomix 600 mixing head with 40 cm^3 mixing volume. Mixing was carried out at 160 °C and 50 rpm for 8 min. Thin films about 120 μm thick of *m*C8-91, *m*C8-87, and the blends were compression molded. The polymer was sandwiched between Mylar sheets and heated to 190 °C for 5 min under minimal pressure before the pressure was sequentially increased to 2 MPa for 5 min and to 5.5 MPa for 1 min. The films were air quenched.

Composition of the copolymers as average branch content and molecular weight data given in Table 1 were provided by the manufacturers. Densities were measured in a 2-propanol−distilled water density gradient column calibrated with glass floats. The melting temperature and heat of melting were obtained on blown films and compression molded films with the Rheometrics DSC using a heating rate of 10 °C min^{-1}.

Methods. The apparatus for sequentially sealing and peeling two film surfaces at the same temperature in the melt was described previously, as were the procedures for preparation of film specimens adhered to a Mylar backing.[16] The seal time was varied from 0.5 to 25 s, and peel rates of 50 and 500 mm min^{-1} were used. The peel strength was calculated as $2P/w$ where P is the measured peel force and w is the specimen width.

Specimens for melt adhesion tests were prepared from molded films in the same manner as blown films. Comparison

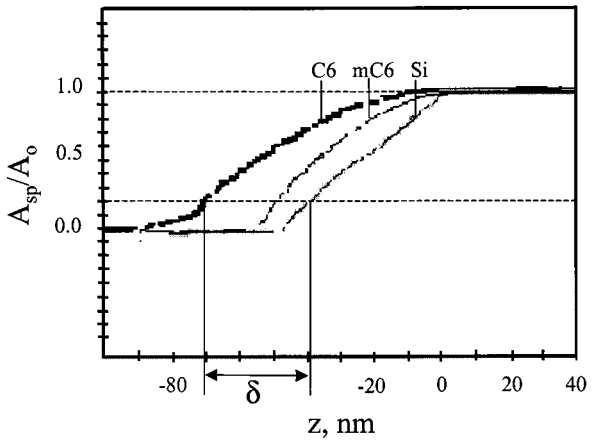

Figure 1. Set point ratio (A_{sp}/A_o) as a function of z for C4, *m*C6, and silicon wafer. Data were obtained with $A_o = 60$ nm.

of peel specimens from blown film with peel specimens from compression molded film of the same polymer was required to ensure that the compression molded surface reproduced the melt adhesion characteristics of the blown film surface. The comparison was made with the 4MP1 copolymer. The peel curves of blown and compression molded films superposed in tests at 130 °C and 500 mm min^{-1}.

Atomic force microscopy (AFM) was conducted in air at ambient conditions using the Nanoscope IIIa multimode head from Digital Instruments (Santa Barbara, CA). Experiments were conducted in the tapping mode using Si probes with 50 N m^{-1} spring constant and resonance frequencies in the range 284−362 kHz. The tip had a radius of 10 nm. The inner surface of blown films was imaged directly. Phase and height images were recorded simultaneously. The interaction of the tip with the specimen was varied from light to hard tapping by adjusting the ratio of the set point amplitude (A_{sp}) to the free oscillation amplitude (A_o). Light tapping phase images (e.g., $A_o = 20$ nm, $A_{sp}/A_o = 0.9$) provided topographical information.[17] Moderate or "normal" tapping conditions (e.g., $A_o = 30-40$ nm, $A_{sp}/A_o = 0.5-0.7$) were sensitive to local stiffness variations. Phase images distinguished stiffer crystalline regions from surrounding amorphous material. Harder tapping increased the depth to which structural features were resolved.

In the force-probe method, the lateral position of the tip was fixed, and the amplitude of the oscillating cantilever was measured as a function of the tip−specimen distance (z).[18] The free oscillation amplitude (A_o) was maintained constant, and the set point amplitude (A_{sp}) was recorded as a function of distance (z) in these experiments. Typical plots of set point ratio (A_{sp}/A_o) as the tip moved closer to the specimen (decreasing z) for C6, *m*C6, and a silicon wafer are displayed in Figure 1. The point of deviation from $A_{sp}/A_o = 1$ was taken as the initial tip−specimen contact ($z = 0$). As z decreased further, A_{sp}/A_o decreased linearly for the rigid silicon wafer. Curvature and a more gradual decrease of A_{sp}/A_o for the film specimens indicated that the tip penetrated into the specimen. The penetration depth (δ) was taken as the difference between the z position of the silicon wafer and the z position of the film specimen at a specific set point ratio. To establish the penetration depth as a function of A_o, δ was recorded at $A_{sp}/A_o = 0.2$.[18] The penetration depth for specific phase images was determined using the imaging values of A_o and A_{sp}/A_o.

To image the bulk of blown films, the film was embedded in epoxy, microtomed using the Ultramicrotome (MT6000-XL) from RMC (Tucson, AZ), and etched in a 0.5 wt % solution of potassium permanganate in a mixture of sulfuric acid and orthophosphoric acid (2:1) for 1 h.[19]

To prepare compression molded surfaces for AFM, the Mylar sheets used for compression molding were rinsed in THF to remove contamination and dried for several hours. The molded surfaces were imaged directly. For images of the bulk of compression molded films, thin sections were cryomicrotomed and imaged directly. Hard tapping was used to image the bulk.

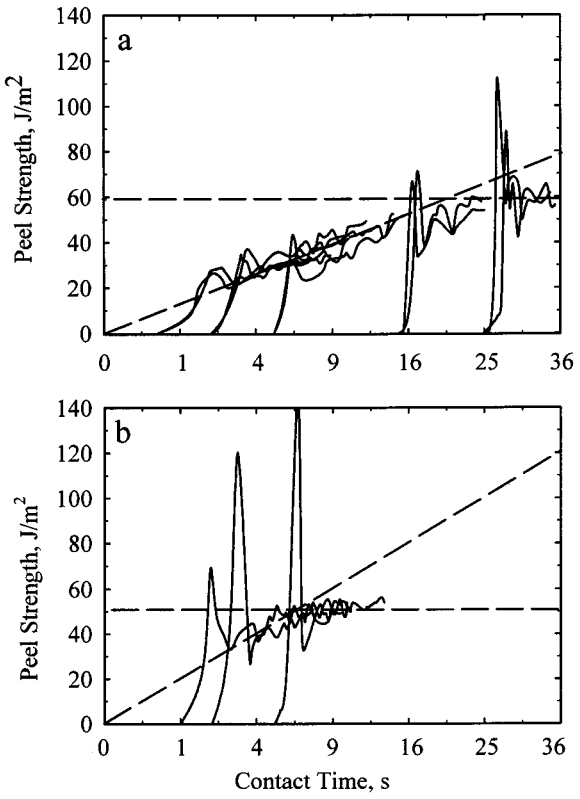

Figure 2. Melt peel curves of blown film obtained at 135 °C with a peel rate of 500 mm min^{-1} for various sealing times plotted as a function of total contact time (t). The time axis is linear with $t^{1/2}$: (a) 4MP1 and (b) C4.

Typically, the higher modulus material appeared light in the AFM phase images and the lower modulus material appeared dark. This was sometimes reversed with hard tapping.[20]

Results and Discussion

Melt Adhesion of Homogeneous and Heterogeneous Copolymers. Melt peel curves for 4MP1 and C4 illustrate the results that were obtained for heterogeneous copolymers (Figure 2). The C6 copolymer exhibited the same behavior as 4MP1 at all experimental conditions tested. The data in Figure 2 were obtained at 135 °C for various seal times with a peel rate of 500 mm min^{-1}. After an initial sharp increase in peel strength as the crack initiated, the peel strength continuously increased during propagation of the peel crack, unlike conventional peel curves where the crack propagates with constant strength after initiation. When the peel strength was plotted as a function of total contact time, i.e., the sum of the seal time and the peel time, the peel curves for different seal times overlapped.

The best power fit of the experimental time dependence with zero intercept was a $t^{1/2}$ dependence at short contact times. At longer times, the peel strength reached a maximum and time-independent value (t^0 dependence). The time to saturation was significantly longer for 4MP1 (and C6) than for C4. As seen in Figure 2, the saturation times at 135 °C were 18 and 7 s, respectively. Another feature that distinguished C4 was a characteristic initial overshoot in the peel curves that significantly exceeded the intrinsic force fluctuations during peeling. The overshoot was not as prominent in the peel curves of 4MP1 (and C6) at short sealing times; however, it appeared with gradually increasing prominence as the seal time approached the saturation time.

The observed $t^{1/2}$ dependence of the peel strength is normal for interdigitation of chains with randomly distributed chain ends.[1] The time dependence should saturate at the maximum (cohesive) strength when the chain completely escapes from the original tube and all the surface chain ends reach the interface. This corresponds to the time that is needed for the entire chain to diffuse the distance of approximately a coil dimension. However, a serious problem develops when the saturation time in peel strength (t_s), 18 s for 4MP1 and C6 at 135 °C, is compared with the surface chain interdigitation time (τ_i). The latter is estimated from the diffusion coefficient D as $\tau_i = R_g^2/4D$, where R_g is the radius of gyration of the polymer coil, to be $\tau_i \cong 5 \times 10^{-2}$ s at 135 °C for chains of the weight-average molecular weight.[16] This is about 400 times less than the time $t_s \cong 18$ s to reach the maximum peel strength at this temperature.

The discrepancy in the interdigitation time was attributed to the existence of a surface layer that the bulk chains needed to diffuse through in order to achieve the maximum adhesion strength. This implied that the surface layer was inert in terms of adhesion; i.e., when the two surface layers were brought together in the melt, they were not capable of developing good tack. This was possible if the surface layer originated from surface segregation of the lower molecular weight, higher branch content fraction of the material. The saturation time was shorter, and the amorphous surface layer correspondingly thinner, for the less heterogeneous C4. Estimates from t_s and the diffusion coefficient for polyethylene were 280 nm for 4MP1 and C6 and 170 nm for C4.[16] The thickness of the amorphous surface layer on the free film was one-half, or 140 nm for 4MP1 and C6 and 85 nm for C4. Despite differences in time behavior, the saturation values of peel strength were practically the same for all heterogeneous copolymers studied.

The postulated surface layer should not exist on films of metallocene copolymer with homogeneous comonomer content and narrower molecular weight distribution. In the absence of an amorphous surface layer, through which the bulk chains must diffuse to reach the interface, maximum adhesion strength should be achieved instantly on the time scale of the peel experiment, and the peel crack should propagate with almost constant force. Indeed, this was observed for the homogeneous copolymer, *m*C6. Figure 3 presents peel curves obtained in tests of *m*C6 at different temperatures above the melting point (117 °C) at a peel rate of 500 mm min^{-1}. The peel crack propagated with constant strength (t^0 dependence), consistent with a fully adhered interface. No time dependence of the peel strength was observed over the entire range of temperatures. (Tests at temperature above 155 °C resulted in tearing fracture.)

Lacking low molecular weight fractions with high branch content, a surface layer with composition different from the bulk was not possible and homogeneous copolymers achieved full adhesion instantly on the time scale of the experiment. Even if lower molecular weight chains concentrated at the surface, the composition of the surface chains would have been the same as the bulk, and the relatively narrow molecular weight distribution of homogeneous copolymers ensured that surface chains would be long enough to produce adhesion strength. The time dependence of adhesion strength would have arisen from diffusion of surface chains and

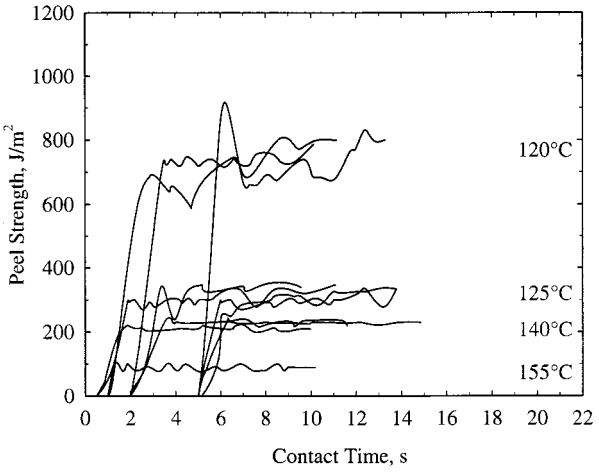

Figure 3. Melt peel curves of *m*C6 blown film obtained at various temperatures with a peel rate of 500 mm min^{-1} for various sealing times plotted as a function of total contact time (t).

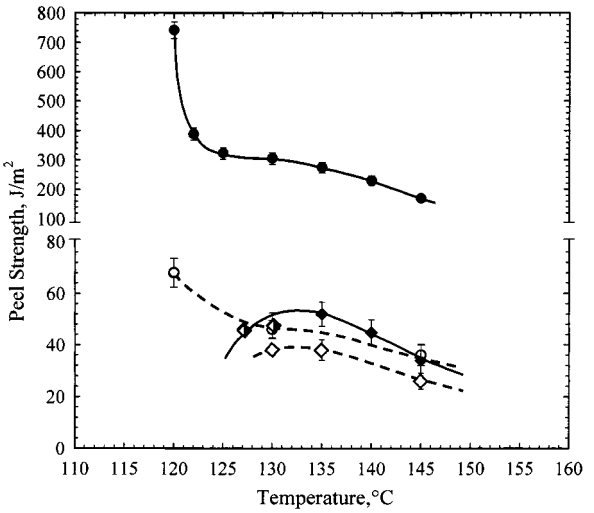

Figure 4. Temperature dependence of the 9 s isochronal melt peel strength of C4 (◆, ◇) and *m*C6 (●, ○) blown films. Solid lines at 500 mm min^{-1}: solid symbols indicate no time dependence; half-solid symbols indicate $t^{1/2}$ dependence. Dashed lines at 50 mm min^{-1}: open symbols, no time dependence.

would have occurred on a much shorter time scale than the experimental time scale.

In addition to the difference in time dependence, the homogeneous copolymer film also exhibited a peel strength that was considerably higher than the fully adhered peel strength of heterogeneous copolymers. The adhesion strength of homogeneous and heterogeneous copolymers at different temperatures and peel rates is summarized in Figure 4. Because the peel strength of heterogeneous copolymers at the high strain rate was time-dependent at short contact times, comparison of *m*C6 with a heterogeneous copolymer C4 was based on the isochronal adhesive strength at a total contact time of 9 s. Above 135 °C, this was sufficient time to achieve full adhesion, and comparison of *m*C6 and C4 showed an almost order of magnitude difference in peel strength. Below 135 °C, full adhesion of C4 films was not achieved in 9 s, and the decrease in adhesion strength approaching the melting temperature reflected the decreasing diffusion rate of long chains through the surface layer. In fact, peel measurements close to the melting temperature magnified the contrast between *m*C6 and C4. In attempts to perform a peel measurement of C4 at

the melting temperature, the specimen fell apart because the low molecular weight amorphous surface layer was incapable of developing good adhesion, and anchoring of long chains in incompletely melted crystallites hampered their diffusional mobility through the surface layer. However, in the absence of a surface layer, adhesion of homogeneous copolymer was possible in the melting range. In this case, the maximum strength was much higher than in the melt because of partial crystallization of the interdigitated chains.

At a lower peel rate of 50 mm min^{-1}, the large difference in peel strength between homogeneous and heterogeneous copolymers ceased, and all the copolymers exhibited similar values of the maximum strength. This was expected for copolymers of similar average molecular weight. The range of strain rates at the crack tip put the melt close to the region of the rubbery plateau, where the elastic component in the viscoelastic response dominated, and stress in the extensional flow was determined mainly by deformation of the entanglement network.[16] It follows qualitatively that the value of the maximum peel strength at a strain rate that exceeds the temperature-dependent relaxation rate should be determined by the plateau modulus, which is practically the same for all linear polyethylenes. Because the copolymers had nearly the same average molecular weight, all of them achieved the rubbery plateau region at the same strain rate, and the maximum melt adhesion strength was the same at each temperature. Thus, the enormous peel rate effect for homogeneous *m*C6 had to be explained from a different position.

Melt adhesion measurements were performed at temperatures well below the melting temperature of extended chain polyethylene crystals at 145−160 °C.[21] Probably, strain-induced crystallization in the elongational strain field at the crack tip accounted for the high peel strength measured for *m*C6 at 500 mm min^{-1}. Strain crystallization relies on chain orientation,[22,23] which is favored by high strain rates, and also depends on comonomer distribution because short chain branches are excluded from the crystal. With homogeneous comonomer distribution, *m*C6 should strain crystallize more readily than the heterogeneous copolymers with low molecular weight, highly branched fractions. The heterogeneous copolymers would require a higher deformation rate to strain crystallize. Indeed, the characteristic stress overshoot in peel curves of C4 at 500 mm min^{-1} (Figure 2b) was attributed to strain crystallization under the higher strain rate at crack initiation.

Surface Morphology. An amorphous surface layer, formed in the melt during blown film fabrication, ought to be preserved during subsequent solidification. A very thin, soft layer should be detectable if the surface is probed very gently. The sequence of AFM phase images in Figure 5 shows the surface of C6 film as it was probed with gradually increasing tapping force. The image obtained with the lightest tapping presents a network of dark lines (Figure 5a). With slightly harder tapping, the dark lines begin to disappear, as seen in the lower left corner of Figure 5b. With normal tapping, most of the dark lines vanish, and some higher modulus crystalline lamellae appear as bright lines on the right side of the image (Figure 5c). Hard tapping enhances the contrast between bright lamellae and large, featureless interlamellar regions of soft amorphous material (Figure 5d). Taken in sequence, the images suggest a surface

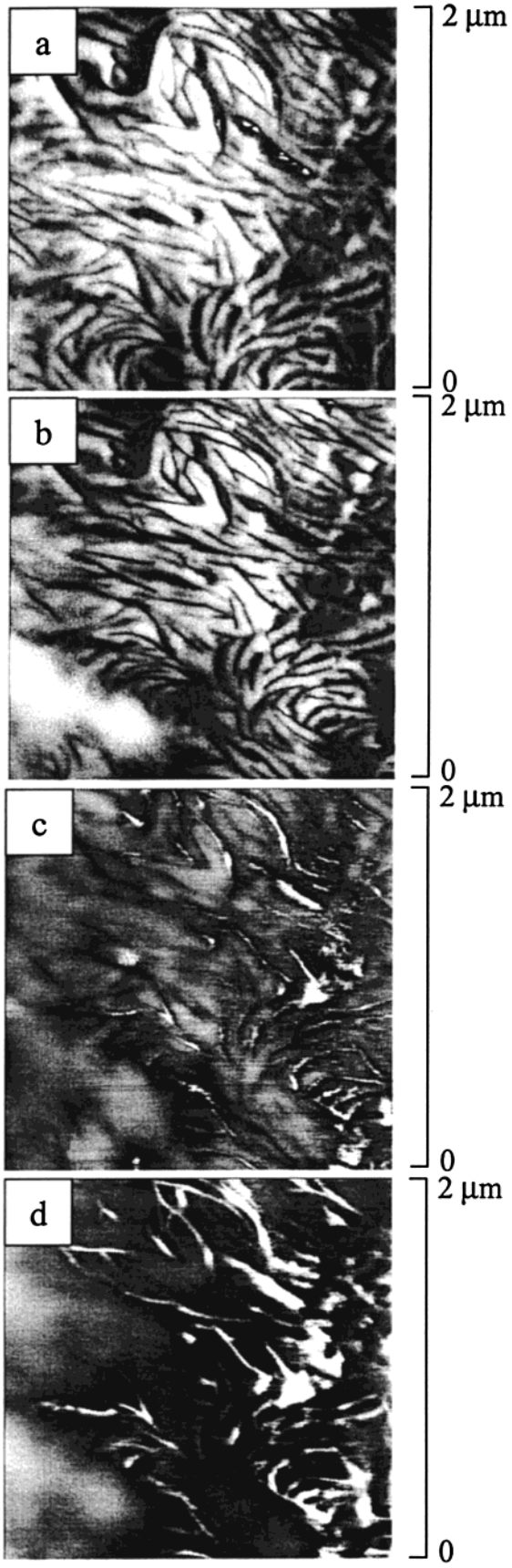

Figure 5. AFM phase images of C6 blown film surfaces: (a) $A_o = 40$ nm, $A_{sp}/A_o = 0.92$, $\delta = 9$ nm; (b) $A_o = 40$ nm, $A_{sp}/A_o = 0.88$, $\delta = 15$ nm; (c) $A_o = 40$ nm, $A_{sp}/A_o = 0.72$, $\delta = 20$ nm; and (d) $A_o = 60$ nm, $A_{sp}/A_o = 0.40$, $\delta = 30$ nm.

enriched in amorphous fractions. These fractions constitute a soft layer through which the AFM tip must

probe in order to detect underlying crystalline lamellae.

A lower free oscillation amplitude (A_o), with similar set point ratios (A_{sp}/A_o), was used to obtain the series of phase images of C4 in Figure 6. Very light tapping of C4 film produced an image with a network of dark lines like that in the corresponding image of C6 (compare Figure 6a with Figure 5a). Slightly harder tapping removed some of the features (Figure 6b). However with C4, the conditions used to obtain Figure 6b revealed some bright lamellae at the bottom the image. Decreasing A_{sp}/A_o to normal tapping showed a denser network of lamellae than the corresponding image of C6 (compare Figure 6c with Figure 5c). However, even with C4, the lamellae were isolated and separated by dark regions of amorphous material. Harder tapping exposed no additional features (Figure 6d).

The height image of C6 in Figure 7, corresponding to the phase image in Figure 5c, was typical of C6 and C4 surfaces. The bright lamellae in the phase image were apparent as dark lines on the right side of the height image. The large light and dark regions were produced by surface undulations, which were also apparent in the section scan. Otherwise, the surface was smooth with no features on the nanometer size scale.

The tip did not probe deeply enough to detect the densely packed lamellae that characterize the bulk morphology of C6 (Figure 8). Rather, as the tip probed more deeply, it encountered individual lamellae separated by amorphous regions. The images suggested a compositional gradient, in accordance with the change in morphology from an almost completely amorphous surface, through a region of isolated crystalline lamellae, before reaching the densely packed lamellar bulk. However, the differences evident in a comparison of Figure 5b,c with Figure 6b,c as well as in the lighter tapping conditions needed to obtain surface images of C4 indicated that the gradient surface layer was thinner on C4 film than on C6 film.

For comparison, *m*C6 film was imaged with tapping conditions similar to those used to obtain Figures 5 and 6. Even the image obtained with the lightest tapping showed striking differences. Instead of a network of dark edge lines that characterized the amorphous surface layer of C6 and C4, the surface of *m*C6 had the texture of closely packed lamellae (Figure 9a). The lamellar texture detected with very light tapping was confirmed when slightly harder tapping exposed densely packed bright lamellae (Figure 9b). Normal and hard tapping revealed no additional structural features (Figure 9c,d). The surface images of *m*C6 film exhibited the lamellar morphology typical of ethylene copolymers.[24] This film did not possess the amorphous surface layer detected on C4 and C6 films.

Densely packed lamellae were clearly distinguished in the height image of *m*C6 in Figure 10, which corresponds to the phase image in Figure 9c. The bright lamellae appeared to be protruding from the surface. The lamellar morphology of *m*C6 produced a much rougher surface than the amorphous material on the surface of C6 (compare Figure 10 with Figure 7). The section analysis revealed that the surface roughness was on the lamellar size scale of about 10 nm.

Tapping conditions (A_o and A_{sp}) could not be used directly to compare phase images in terms of actual penetration depth because the tip−specimen interaction was not the same from one copolymer to another. Identical tapping conditions gave deeper penetration on a more compliant surface. To obtain the actual penetration depth, the force-probe method was used. Penetra-

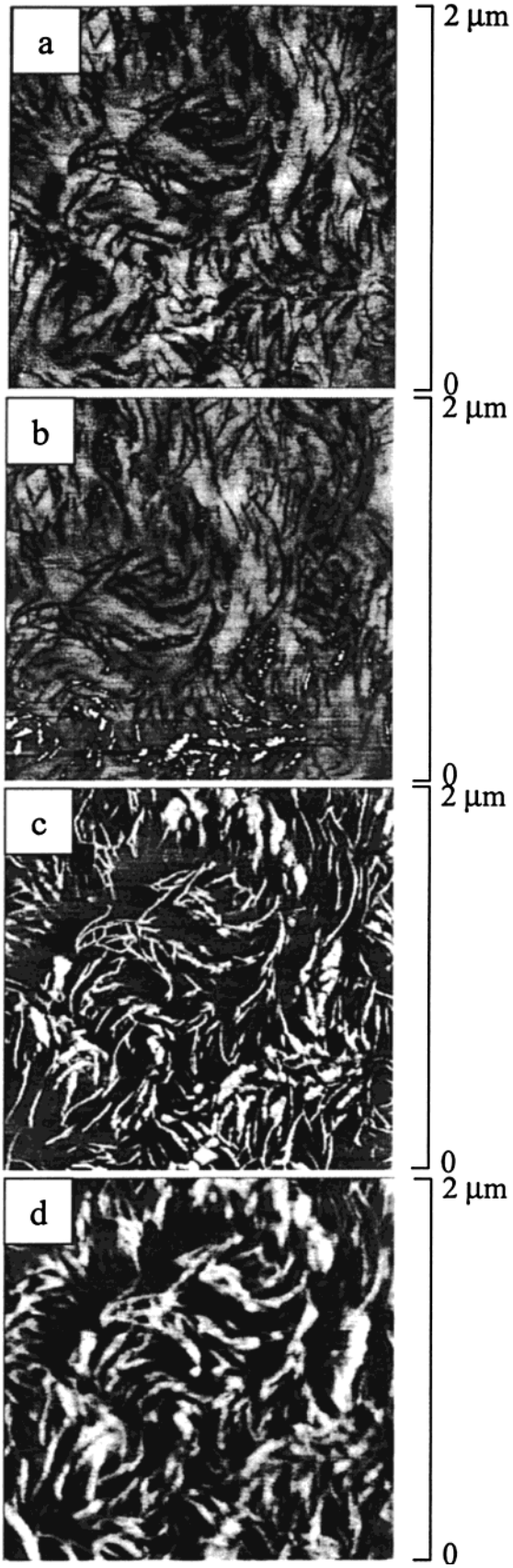

Figure 6. AFM phase images of C4 blown film surfaces: (a) $A_o = 21$ nm, $A_{sp}/A_o = 0.95$, $\delta < 1$ nm; (b) $A_o = 21$ nm, $A_{sp}/A_o = 0.92$, $\delta = 4$ nm; (c) $A_o = 21$ nm, $A_{sp}/A_o = 0.73$, $\delta = 17$ nm; and (d) $A_o = 57$ nm, $A_{sp}/A_o = 0.50$, $\delta = 25$ nm.

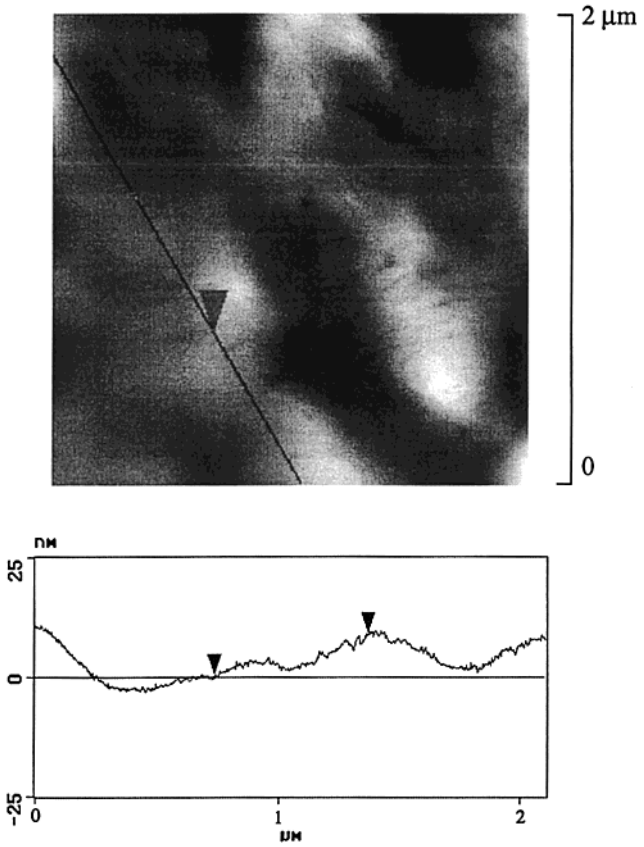

Figure 7. AFM height image of C6 corresponding to the phase image in Figure 5c with section scan.

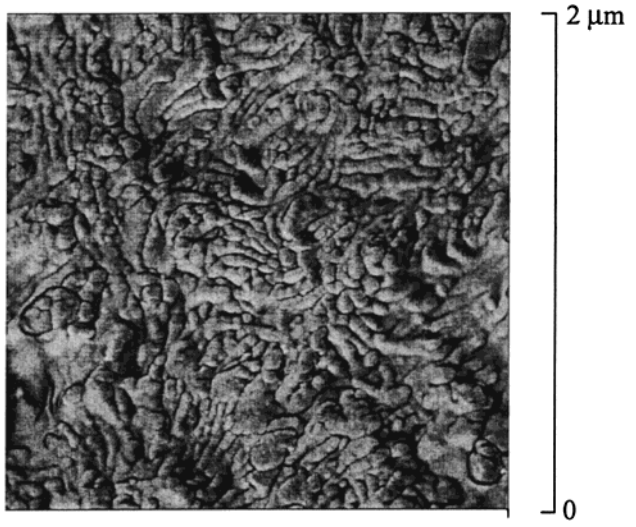

Figure 8. Phase image of the bulk of C6 blown film.

tion depth (δ) obtained in this way is shown in Figure 11 as a function of free oscillation amplitude, which is proportional to the maximum imposed force. As the tip force increased, the tip penetrated deeper into the surface. In the initial part of the curves, the penetration depth increased rapidly with increasing A_o. The plateau at higher A_o indicated a limit to the penetration depth achievable with the particular cantilever.

The heterogeneous copolymer films C4 and C6 exhibited similar curves with a maximum penetration depth of 30−40 nm. This value was comparable to that measured on typical elastomers with similar probe conditions.[18] The elastomer-like response of C4 and C6 indicated an amorphous surface layer that was thicker than the penetration depth of the probe. This meant

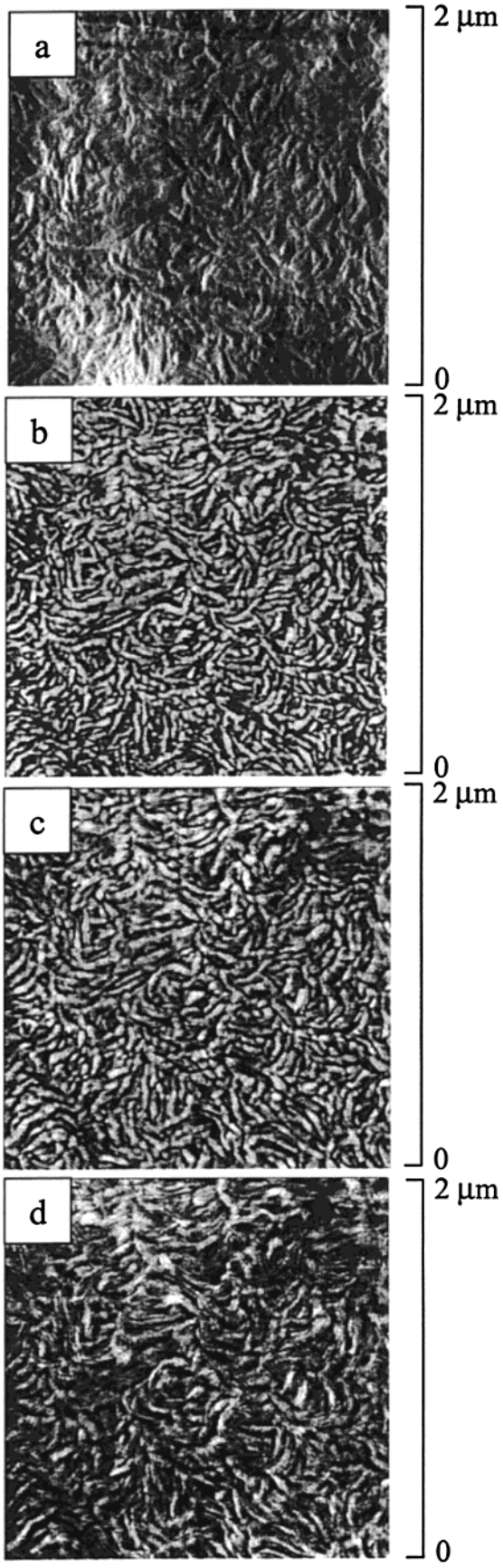

Figure 9. AFM phase images of *m*C6 blown film surfaces: (a) $A_o = 32$ nm, $A_{sp}/A_o = 0.95$, $\delta < 1$ nm; (b) $A_o = 32$ nm, $A_{sp}/A_o = 0.90$, $\delta = 3$ nm; (c) $A_o = 42$ nm, $A_{sp}/A_o = 0.50$, $\delta = 10$ nm; and (d) $A_o = 97$ nm, $A_{sp}/A_o = 0.40$, $\delta = 10$ nm.

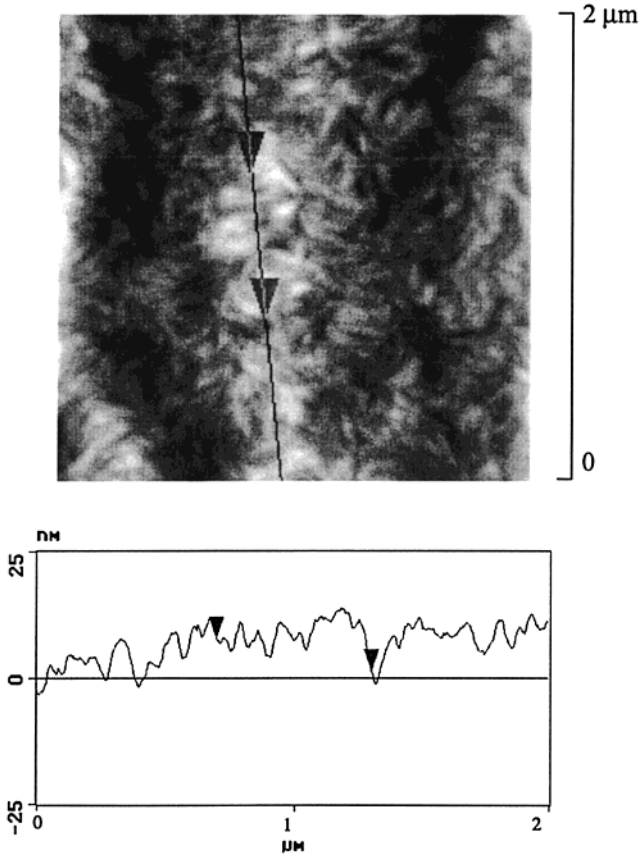

Figure 10. AFM height image of *m*C6 corresponding to the phase image in Figure 9c with section scan.

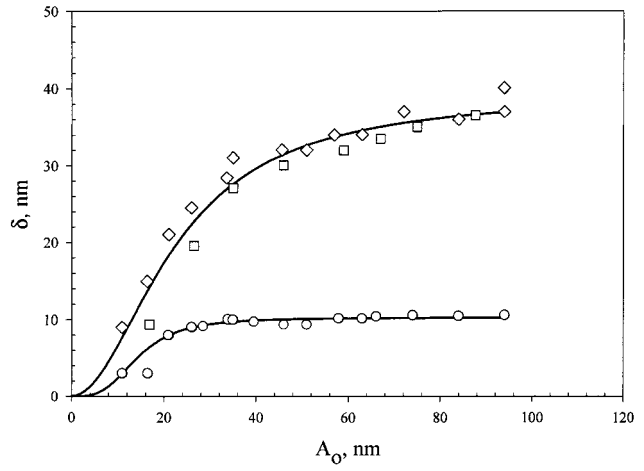

Figure 11. Indentation depth (δ) taken at $A_{sp}/A_o = 0.20$ as a function of free oscillation amplitude (A_o) for C6 (□), C4 (◇), and *m*C6 (○) blown film.

that tip penetration of the surface was not affected by the underlying crystalline bulk, nor was it significantly affected by isolated lamellae in the surface layer, which were revealed by phase images to be more numerous and closer to the surface of C4 than C6. In such a material, penetration depth depended on the competition between attractive tip−specimen interactions, which dominated at small indentations (<30 nm), and repulsive forces, which dominated at larger indentations (>30 nm).[18] Thus, amorphous surface layer could have been much thicker than 30−40 nm, which was consistent with the estimated depth of about 100 nm. The surface of *m*C6 was markedly less penetrable. After reaching a depth of 10 nm, the tip did not penetrate further. The plateau depth was remarkably constant, in contrast to the gradual increase in plateau depth of C4 and C6.

The images in Figures 5 and 6 can now be considered in terms of gradually increasing penetration depth as indicated in the figure captions. With minimal tip penetration, the phase images showed primarily topological features. The dark lines in Figures 5a and 6a were predominately edges where the height changed;[24] they were equivalent to fractographic level difference lines.[25] Possibly, some of the thicker dark streaks were lamellae that projected from the surface. With increasing penetration depth, the edge lines started to disappear, as in the lower left corner of Figure 5b, until most of the topological features vanished (Figure 5c). At a penetration depth of about 20 nm for C6, the bright lines in Figure 5c revealed isolated, higher modulus, crystalline lamellae. Correspondence between bright lamellae in Figure 5c and specific topological lines in Figure 5a,b identified the latter as projecting lamellae. Deeper penetration to 30 nm further enhanced the contrast between lamellae and large, featureless interlamellar regions of soft amorphous material (Figure 5d).

The pattern was totally consistent with a surface enriched in amorphous material. This material constituted a soft layer through which the AFM tip had to probe. The layer was too thick, estimated to be on the order of 100 nm from seal kinetics, for the probe to reveal the underlying bulk morphology. However, by detecting the presence of some crystalline lamellae, the phase images suggested a gradient of increasing lamellar density. Qualitatively, the surface characteristics of C4 and C6 were the same, with the most significant differences being a larger number of lamellae imaged on the C4 surface and consistently smaller penetration depths required to obtain comparable images to C6. The differences corroborated the thinner amorphous layer postulated for C4 from the seal kinetics. The *m*C6 surface was strikingly different. Much lower penetration depths were achieved, not more than 10 nm. Furthermore, phase images and height images exhibited essentially the same features of a close-packed lamellar morphology regardless of penetration depth. The surface was essentially the same as the bulk in composition and morphology and did not possess the amorphous surface layer detected on C4 and C6 films.

Homogeneous Copolymers of Different Branch Content. Two homogeneous octene copolymers were studied for the effect of branch content on melt adhesion. One of them (*m*C8-91) resembled *m*C6 in branch content, crystallinity, and melting temperature. The melt surfaces and melt adhesion behavior of *m*C6 and *m*C8-91 were expected to be comparable except for differences arising from the method of film preparation. Indeed, AFM phase images of the *m*C8-91 compression molded film surface revealed a closely packed lamellar morphology (Figure 12a) that closely resembled the surface of *m*C6 blown film (compare with Figure 9). With higher comonomer content than *m*C8-91, homogeneous *m*C8-87 formed fringed micellar crystals that appeared as a granular texture in transmission electron micrographs and tapping mode AFM phase images of the bulk.[26−28] The combination of the granular texture of fringed micellar crystals and the imprint texture of the Mylar molding surface probably produced the uneven texture of *m*C8-87 compression molded surfaces in Figure 12b.

In all peel curves of *m*C8-91, the time to crack initiation exceeded the characteristic time for full adhe-

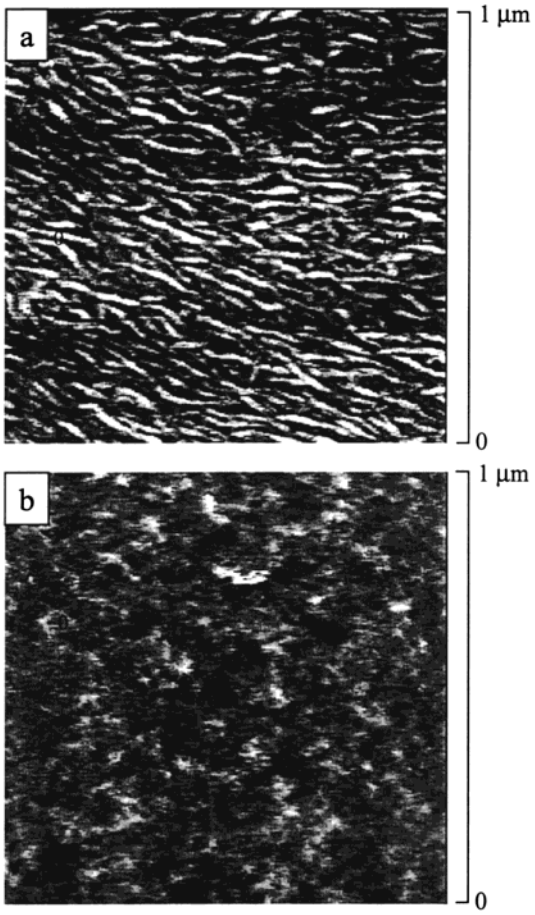

Figure 12. AFM phase images of compression molded film surfaces: (a) *m*C8-91 and (b) *m*C8-87.

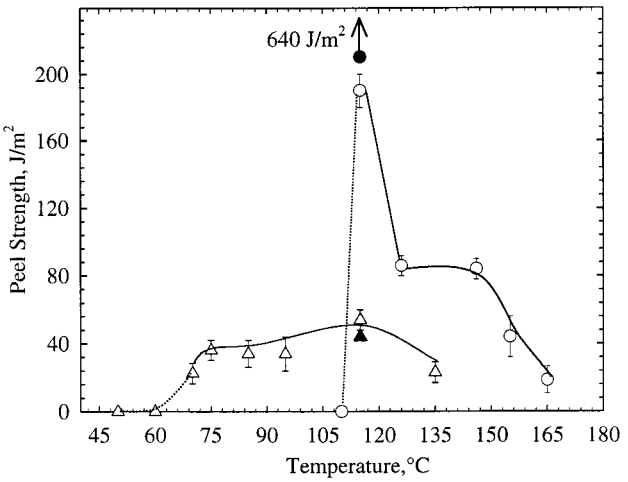

Figure 13. Temperature dependence of the melt peel strength of *m*C8-91 (●, ○) and *m*C8-87 (▲, △) compression molded films. Solid points obtained at 500 mm min^{-1}; open points obtained at 50 mm min^{-1}: all with no time dependence.

sion and constant peel strength (t^0 dependence) was recorded. At the lower peel rate, 50 mm min^{-1}, the adhesion strength of *m*C8-91 decreased with peel temperature in accordance with a fully adhered interface (Figure 13). As expected, *m*C8-91 closely resembled *m*C6 in temperature dependence and magnitude of adhesion strength (compare with Figure 4). Attempts to measure melt adhesion of compression molded films at the higher peel rate of 500 mm min^{-1} resulted in tearing fracture at temperatures above 115 °C. Probably, compression molded films did not have the film strength of oriented blown films. Therefore, the effect of peel rate was illustrated with a single point for 500 mm min^{-1} at 115 °C. The higher rate produced a dramatic increase in peel strength from 200 to 640 J m^{-2}. The strong rate effect, attributed to strain crystallization, further strengthened the correspondence between compression molded film of *m*C8-91 and blown film of *m*C6 in terms of melt surfaces and melt adhesion.

Like the other homogeneous copolymers, films of *m*C8-87 achieved full adhesion instantly on the experimental time, and the t^0 dependence of peel strength was recorded. The low melting temperature of homogeneous *m*C8-87 resulted in measurable adhesion at temperatures as low as 70 °C (Figure 13). Increasing the peel rate from 50 to 500 mm min^{-1} had almost no effect on the peel strength, demonstrating that the high branch content prevented strain crystallization. The adhesion strength was comparable in magnitude to that of heterogeneous copolymers of similar molecular weight (compare with Figure 4) as expected for a melt in the region of the rubbery plateau where stress is determined mainly by the elastic response of the entanglement network. The result supported the previous conclusion that the average chains of a heterogeneous copolymer created adhesion strength, and the time dependence was due to diffusion of average chains through an amorphous surface layer and not to extremely slow diffusion of a minor fraction of ultrahigh molecular weight chains present in the broad molecular weight distribution.

With similar molecular weights, the primary difference between *m*C8-91 and *m*C8-87 was the possibility for strain crystallization at the higher peel rate. Whereas the high branch content of *m*C8-87 prevented crystallization of oriented chains under the experimental peel conditions, the ability of *m*C8-91 to readily strain crystallize was exploited to reveal effects of surface composition on melt adhesion of blends prepared from homogeneous copolymers of different branch content.

Blends of Homogeneous Copolymers. The surface layer of heterogeneous copolymers was experimentally modeled by blending *m*C8-87 having high concentration of short-chain branches with *m*C8-91 having low concentration of short-chain branches. At micron-scale resolution, film surfaces of compression molded blends with 10% and 30% *m*C8-87 appeared homogeneous with no evidence of phase-separated domains. At higher resolution, the surface of the blend with 10% *m*C8-87 exhibited a lamellar texture (Figure 14a). The larger separation and poorer organization of the lamellae compared to the *m*C8-91 surface (compare with Figure 12a) suggested that the surface was enriched with *m*C8-87. In contrast, the surface of the blend with 30% *m*C8-87 in Figure 14b exhibited the same granular texture as the *m*C8-87 surface (compare with Figure 12b). The absence of lamellae indicated that the 30% *m*C8-87 blend possessed a surface layer of the more highly branched copolymer. The copolymers differed enough in comonomer content that the 30% *m*C8-87 blend might have been phase-separated.[29,30] Indeed, AFM images of the bulk clearly showed two phases with domains of *m*C8-87 distributed in the *m*C8-91 continuous phase (Figure 14c). The reverse contrast, with the *m*C8-91 continuous phase appearing dark and the dispersed *m*C8-87 domains appearing light, was due to the hard tapping used to obtain this image.[24]

Unlike the highly branched fractions of heterogeneous copolymers, the molecular weight of *m*C8-87 was high

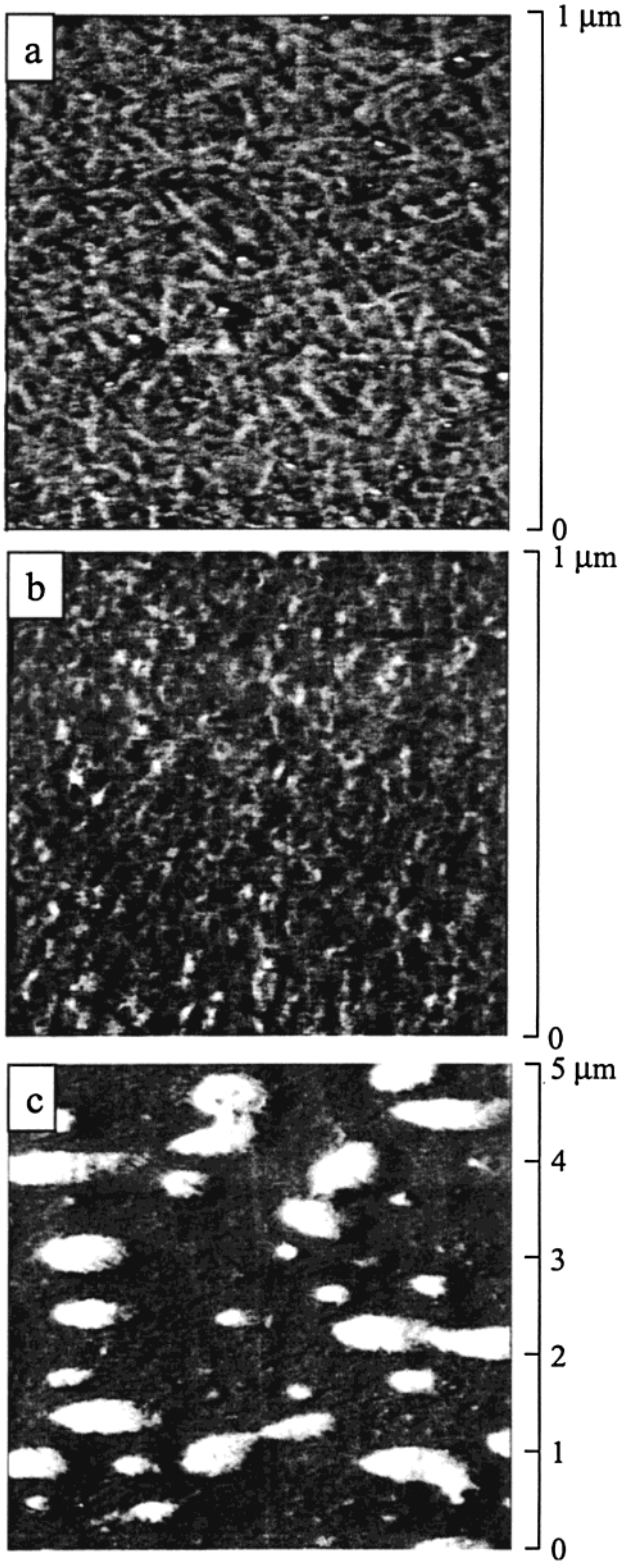

Figure 14. AFM phase images of compression molded *m*C8-87/*m*C8-91 blend films: (a) surface of the blend with 10 vol % *m*C8-87, (b) surface of the blend with 30 vol % *m*C8-87, and (c) bulk of the blend with 30 vol % *m*C8-87.

enough that entanglements of interdiffused surface chains imparted full adhesion instantly on the experimental time scale. Therefore, an effect of surface composition on peel strength was anticipated under testing conditions that promoted strain crystallization, specifically at the higher peel rate where strain crystallization of *m*C8-91 resulted in a large difference in peel strength between *m*C8-91 and *m*C8-87. Therefore, the adhesion strength of the blends was evaluated at 500 mm min^{-1} and 115 °C. (Higher temperatures resulted in tearing fractures at this peel rate.) The high peel rate had the additional possibility for detecting increases in strain-crystallizable fractions at the surface on the time scale of the experiment, for example, by diffusion of *m*C8-91 through a surface layer enriched in *m*C8-87.

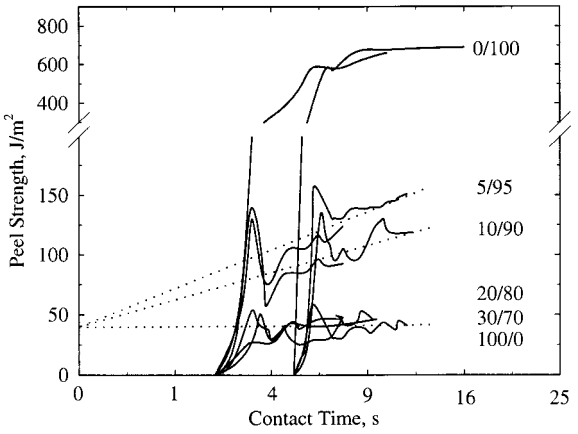

Figure 15. Melt peel curves of *m*C8-91, *m*C8-87, and their blends obtained at 115 °C with a peel rate of 500 mm min^{-1} for sealing times of 2 and 5 s plotted as a function of total contact time (t). The time axis is linear with $t^{1/2}$. The blend composition is indicated as *m*C8-87/*m*C8-91 (vol %/vol %).

Blending with as little as 5% *m*C8-87 decreased the peel strength of *m*C8-91 dramatically (Figure 15). A prominent stress overshoot at crack initiation and a continuous increase in adhesion strength during crack propagation characterized the peel curves of blends with small amounts (5% and 10%) of *m*C8-87 and indeed reproduced the main features in the melt adhesion curves of heterogeneous copolymers (Figure 2). Thus, melt adhesion behavior confirmed evidence from AFM that blends in this composition range possessed a surface enriched in *m*C8-87. The time dependence was attributed to gradual diffusion of *m*C8-91 to the surface. The best power fit with intercept at the peel strength of *m*C8-87 was the $t^{1/2}$ dependence as indicated by the time axis in Figure 15. In contrast, peel curves of blends with 20% or more *m*C8-87 were indistinguishable from the peel curve of *m*C8-87. The peel crack propagated with constant force (t^0 dependence) with the same peel strength as *m*C8-87. The result was consistent with AFM evidence for a surface layer of *m*C8-87. Moreover, it appeared that no significant diffusion of *m*C8-91 through the surface layer occurred on the time scale of the experiment.

By exhibiting the major melt adhesion characteristics of heterogeneous copolymers, including the $t^{1/2}$ dependence at higher peel rate and a stress overshoot at crack initiation, blends of *m*C8-91 with 5 and 10% *m*C8-87 confirmed the concept of a surface layer enriched in highly branched fractions. For both heterogeneous copolymers and blends of homogeneous copolymers, AFM images provided direct evidence of an enriched surface layer. The driving force for surface enrichment of the blends was enthalpic due to the higher branch content of *m*C8-87. The entropic component was negligible because the molecular weight and molecular weight distributions did not differ greatly. Blends with 5 and 10% *m*C8-87 were considered as miscible in the melt. When two surfaces were brought into contact, *m*C8-91 chains diffused to the interface through the

surface layer enriched in *m*C8-87 in a manner completely analogous to the proposed diffusion of average chains through a surface layer enriched in low molecular weight, highly branched fractions in heterogeneous copolymers. However, because both *m*C8-87 and *m*C8-91 chains contributed to adhesion strength, the gradual increase in adhesion strength with time was attributed to strain crystallization of *m*C8-91.

In contrast, the surface layer in blends with 20% and more *m*C8-87 prevented or greatly retarded diffusion of *m*C8-91 chains to the interface. Without the phase diagram for this copolymer pair, it is only speculation that the *m*C8-87-rich surface layer phase-separated from the bulk in these blend compositions. The AFM images confirmed phase separation in the solidified blend. Possibly, the melt adhesion temperature was below the dissolution temperature for this composition. In this case, the surface layer was saturated, there was no driving force toward homogeneity when sealing removed the surface, and the surface layer was essentially impermeable to *m*C8-91.

Conclusions

This study concerned the effect of chain heterogeneity on development of self-adhesion above the melting temperature in short-chain branched polyethylenes. In particular, the study confirmed the existence of an amorphous surface layer on films of heterogeneous ethylene copolymers that was previously postulated to be responsible for the characteristic time dependence for development of melt adhesion. Atomic force microscopy phase images obtained with gradually increasing tapping force revealed a featureless, amorphous surface with isolated subsurface lamellae. The tip did not probe deeply enough to detect the densely packed lamellae that characterize the bulk morphology of ethylene copolymers. Actual penetration depths of the AFM tip were obtained with the force-probe method. By probing to about 30−40 nm, the AFM tip did not penetrate through the amorphous layer, which was previously estimated to be about 100 nm thick.

The amorphous layer on heterogeneous copolymer films was thought to originate from surface segregation of the lower molecular weight, higher branch content fraction of the material. In this respect, the occurrence of the surface layer was inherent for a polymer with heterogeneous molecular composition. The hypothesis was tested by comparison with metallocene copolymers with homogeneous comonomer distribution and narrower molecular weight distribution. Atomic force microscopy confirmed that films of these polymers did not possess a surface layer that was different from the bulk. As a result, the maximum melt adhesion strength developed instantaneously on the experimental time scale as soon as the surfaces were brought into contact. In this case, peeling the adhered interface in the melt was dramatically affected by strain-induced crystallization in the extensional flow at the running crack tip. Blending two homogeneous copolymers of highly different comonomer content resulted in a surface layer similar to that of heterogeneous copolymers. Blends with only 5−10% of a highly branched copolymer reproduced the major melt adhesion characteristics of heterogeneous copolymers.

Acknowledgment. This research was generously supported by BP Amoco Chemicals.

References and Notes

(1) Wool, R. P. *Polymer Interfaces*; Hanser: Munich, 1995.
(2) Jones, R. A.; Richards, R. W. *Polymers at Surfaces and Interfaces*; Cambridge University Press: New York, 1999.
(3) Wild, L. *Adv. Polym. Sci.* **1990**, *98*, 1−198.
(4) Schuman, T.; Stepanov, E. V.; Nazarenko, S.; Capaccio, G.; Hiltner, A.; Baer, E. *Macromolecules* **1998**, *31*, 4551−4561.
(5) Schuman, T.; Nazarenko, S.; Stepanov, E. V.; Magonov, S. N.; Hiltner, A.; Baer, E. *Polymer* **1999**, *40*, 7373−7385.
(6) Roland, C. M.; Bohm, G. G. A. *Macromolecules* **1985**, *18*, 1310−1314.
(7) Von Seggern, J.; Klotz, S.; Cantow, H.-J. *Macromolecules* **1991**, *24*, 3300−3303.
(8) Pearson, D. S.; Fetters, L. J.; Graessley, W. W.; Ver Strate, G.; Von Meerval, E. *Macromolecules* **1994**, *27*, 711−719.
(9) Morgan, R. L.; Hill, M. J.; Barham, P. J.; Frye, C. J. *Polymer* **1997**, *38*, 1903−1909.
(10) Crist, B.; Hill, M. J. *J. Polym. Sci., Part B*: *Polym. Phys.* **1997**, *35*, 2329−2353.
(11) Wu, D. T.; Fredrickson, G. H. *Macromolecules* **1996**, *29*, 7919−7930.
(12) Schaub, T. F.; Kellog, G. J.; Mayes, A. M.; Kulasekere, R.; Ankner, J. F.; Kaiser, H. *Macromolecules* **1996**, *29*, 3982−3990.
(13) Frischknecht, A.; Fredrickson, G. H. *Macromolecules* **1999**, *32*, 6831−6836.
(14) Scheffold, F.; Budkowski, A.; Steiner, U.; Eiser, E.; Klein, J.; Fetters, L. J. *J. Chem. Phys.* **1996**, *104*, 8795−8806.
(15) Brant, P.; Karim, A.; Douglas, J. F.; Bates, F. S. *Macromolecules* **1996**, *29*, 5628−5634.
(16) Qureshi, N. Z.; Stepanov, E. V.; Capaccio, G.; Hiltner, A.; Baer, E. *Macromolecules* **2001**, *34*, 1358−1364.
(17) Magonov, S.; Godovsky, Y. *Am. Lab.* **1999**, *31* (8), 52−58.
(18) Bar, G.; Ganter, M.; Brandsch, R.; Delineau, L.; Wangbo, M.-H. *Langmuir* **2000**, *16*, 5702−5711.
(19) Shabana, H. M.; Olley, R. H.; Bassett, D. C.; Zachmann, H. G. *J. Macromol. Sci., Phys.* **1996**, *B35*, 691−708.
(20) Magonov, S. N.; Elings, V.; Whangbo, M.-H. *Surf. Sci.* **1996**, *375*, L385−391.
(21) Wunderlich, B. *Macromolecular Physics*; Academic: Boston, 1980; Vol. 3.
(22) Mandelkern, L. *Comprehensive Polymer Science*; Pergamon: Oxford, 1989; Vol. 2.
(23) Mackley, M. R.; Keller, A. *Philos. Trans. A* **1975**, 29−66.
(24) Magonov, S. N.; Reneker, D. H. *Annu. Rev. Mater. Sci.* **1997**, *27*, 175−222.
(25) Roulin-Moloney, A. C. *Fractography and Failure Mechanisms of Polymers and Composites*; Elsevier: London, 1989.
(26) Minick, J.; Moet, A.; Hiltner, A.; Baer, E.; Chum, S. P. *J. Appl. Polym. Sci.* **1995**, *58*, 1371−1384.
(27) Bensason, S.; Minick, J.; Moet, A.; Chum, S.; Hiltner, A.; Baer, E. *J. Polym. Sci., Part B: Polym. Phys.* **1996**, *34*, 1301−1315.
(28) Chen, H. Y.; Chum, S. P.; Hiltner, A.; Baer, E. *J. Polym. Sci., Part B*: *Polym. Phys.*, in press.
(29) Bensason, S.; Nazarenko, S.; Chum, S.; Hiltner, A.; Baer, E. *Polymer* **1997**, *38*, 3513−3520.
(30) Wignall, G. D.; Alamo, R. G.; Londono, J. D.; Mandelkern, L.; Kim, M. H.; Lin, J. S.; Brown, G. M. *Macromolecules* **2000**, *33*, 551−561.

MA000584P